4258–4265 *Nucleic Acids Research, 2021, Vol. 49, No. 8* *Published online 13 April 2021*
doi: 10.1093/nar/gkab212

Dynamically elongated associative toehold for tuning DNA circuit kinetics and thermodynamics

Yan Shan Ang and Lin-Yue Lanry Yung*

Chemical & Biomolecular Engineering, National University of Singapore, 4 Engineering Drive 4,117585, Singapore

Received January 06, 2021; Revised March 13, 2021; Editorial Decision March 15, 2021; Accepted April 12, 2021

ABSTRACT

Associative toehold is a powerful concept enabling efficient combinatorial computation in DNA circuit. A longer association length boosts circuit kinetics and equilibrium signal but results in higher leak rate. We reconcile this trade-off by using a hairpin lock design to dynamically elongate the effective associative toehold length in response to the input target. Design guidelines were established to achieve robust elongation without incurring additional leakages. Three hairpin initiators with different combinations of elongated associative toehold (4 → 6 nt, 5 → 8 nt and 6 → 9 nt) were shortlisted from the design framework for further discussion. The circuit performance improved in terms of reaction kinetics, equilibrium signal generated and limit of detection. Overall, the elongated associative toehold served as a built-in function to stabilize and favour the forward, desired reaction when triggered.

INTRODUCTION

Dynamic DNA nanotechnology, or DNA circuit, offers a highly programmable toolbox for designing molecular pathways based on Watson–Crick base pairing (1,2). Different strategies have been employed to trigger the toehold-mediated strand displacement reaction (3–6). One concept is associative toehold where the toehold and branch migration domains are decoupled on separate DNA strands, and later dynamically reassembled into an active unit in response to specific hybridization events (7). This is a powerful concept especially for combinatorial computation where multiple inputs can be evaluated with lesser number of DNA strands and without having to re-synthesize the entire system (8).

This basic design has evolved beyond molecular computing using nucleic acids inputs to the proximity-induced detection of other biomolecule inputs, for example, proteins, protein complexes and cell surface receptors (9–12) or as a strategy for supressing circuit leakage (13). The fundamental principle is based on the drastic increase in local DNA concentration when the separate strands are brought into proximity by target binding, thereby stabilizing the DNA three-way junction for downstream strand displacement reaction. A study by Li *et al.* demonstrated that the duplex length in the associative domain and spacer length are key factors influencing the kinetics of such strand displacement scheme (14). As all domains involved in the basic associative toehold are exposed in single-stranded form and readily available for hybridization (both intended and spurious), we previously reported the importance of tuning the domain lengths, particularly that of the association domain, to minimize circuit leakage (15). These combined observations imply that having a longer associative domain should favour proximity strand displacement with the trade-off of high leakage rate. One workaround design is to use a blocker strand to protect the otherwise exposed domains in duplex form and reduce leakage. However, this adds substantial kinetic barrier which hinders the overall reaction for duplex length longer than 10 – 12 nt (14).

Here, we attempt to reconcile the trade-off between the rates of the desired reaction and undesired leakage necessarily incurred in the conventional proximity-induced strand displacement reaction as both reactions are determined by a single design parameter, that is, the length of associative domain (domain *a*) in the linear initiator (**I1**) (Figure 1A). We propose to expand the design space by introducing two additional domains to the initiator in the form of a hairpin lock (**HP-I1**) (Figure 1B). Specifically, an 'elongation domain' (domain *e*) is sequestered in the stem of the hairpin lock which is further stabilized in its initial 'closed' state by a short 'clamp domain' (domain b_2*), taken from part of the original toehold domain *b** (16,17). In its non-triggered state, the association region is kept short as the length of domain *a* to minimize circuit leakage. When triggered by the proximity-induced binding between initiators **HP-I1** and **I2**, the association region is effectively elongated to the combined lengths of domain *a* + *e* and forms a more stable three-way junction for stronger signal generation. This occurs by the partial opening of the hairpin lock by domain *e** on **I2**, followed by the spontaneous dissociation of the clamp domain b_2* to reveal the remaining toehold domain b_1* in the final 'opened' state.

*To whom correspondence should be addressed. Tel: +65 6516 1699; Fax: +65 6779 1936; Email: cheyly@nus.edu.sg

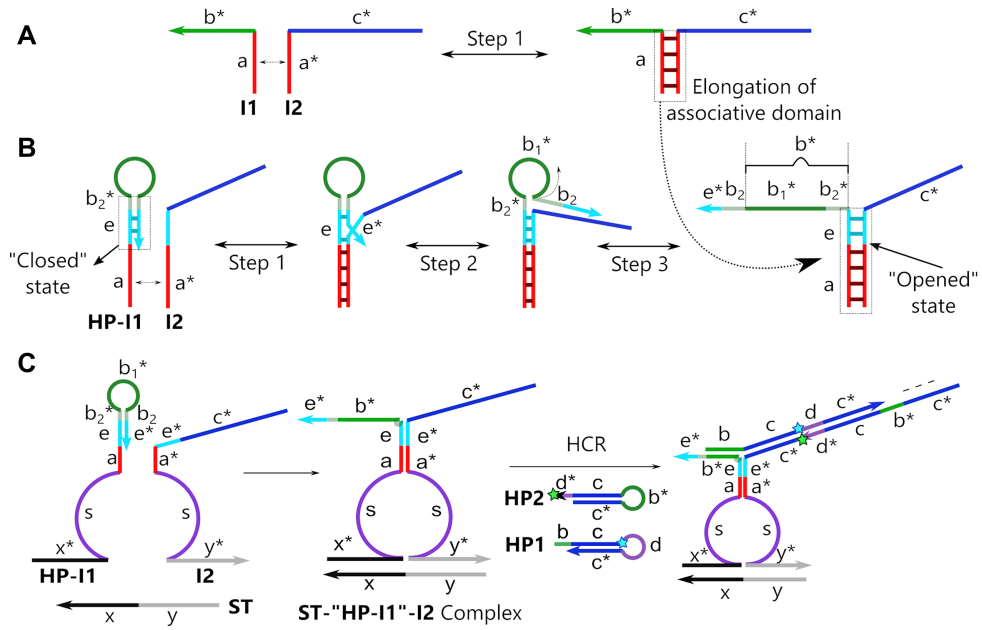

Figure 1. Concept of the dynamically elongated associative toehold. (**A**) The conventional associative toehold design involves the (step 1) hybridization of the association region (domain *a*) on two linear initiator strands (**I1** and **I2**) which stabilizes the assembly of the complete *c* b** trigger strand. (**B**) In our proposed design, the elongation domain *e*, together with a clamp domain b_2*, are sequestered as a hairpin lock ('closed' state) in **HP-I1**. (Step 2) This hairpin lock is then partially displaced by domain *e** on **I2** followed by (step 3) the spontaneous dissociation of domain b_2*. The initial 'closed' state has a shorter association region (domain *a*) with low leak rate; while the final 'opened' state (domain *a* + *e*) is effectively stabilized by a longer association region as a result of this elongation mechanism for stronger signal generation. (**C**) The elongated associative toehold was implemented on our previously reported split proximity circuit (SPC) where two target binding events, mediated by the split target (**ST**), bring the initiators in proximity to trigger the downstream hybridization chain reaction (HCR).

We implemented the elongated associative toehold concept on our previously reported split proximity circuit (SPC) which is based on the principle of proximity-induced strand displacement. A synthetic split target (**ST**) was used to mimic the proximity binding of **HP-I1** and **I2**, facilitated by the binding of complementary recognition domains *x** and *y** (Figure 1C). The SPC was designed to trigger a downstream hybridization chain reaction (HCR) and generate a linearly amplified fluorescence resonance energy transfer (FRET) signal (18).

MATERIALS AND METHODS

Materials

All DNA and RNA oligonucleotides used in this study were purchased from Integrated DNA Technologies (IDT), and HPLC purified by IDT unless otherwise stated. The nucleic acid sequences are shown in Supplementary Table S1 and S2. The lyophilized DNA was reconstituted in 1× Tris–EDTA buffer (1 × TE, pH 8.0) to give ca. 100 μM stock and stored at 4°C for up to a year, except for Cy3/Cy5-modified DNAs which were stored at −20°C and protected from light. The following chemicals were used as received: sodium chloride (NaCl, ≥99.5%) and magnesium chloride ($MgCl_2$, ≥98%) were purchased from Sigma Aldrich. 10× phosphate buffered saline (PBS, pH 7.4) and 1× Tris–ETDA (TE, pH 8.0) was purchased from 1st BASE. Milli-Q water with resistance >18.2 MΩ•cm was used throughout the experiment.

NUPACK analysis

NUPACK web server was used for the design and analysis of nucleic acid structures and systems (19). NUPACK analysis was carried out for *n* number of interacting DNA species at 25°C to form a maximum complex size of *n* strands. The Na^+ and Mg^{2+} concentrations were set as the same values used in the respective experiments.

Preparation of split proximity circuit components

The hybridization chain reaction (HCR) hairpins were prepared just before the experiments. 1 μM of hairpin 1 (**HP1**) tagged with Cy5 and hairpin 2 (**HP2**) tagged with Cy3 was heated separately in 1× PBS (pH 7.4) and 10 mM $MgCl_2$ to 95°C for 5 min and snap-cooled on ice for at least 15 min. Thereafter, the circuit components were mixed in the following sequences to the final reaction concentrations of 20 nM **HP2**, 20 nM **I2**, 20 nM **I1**/**HP-I1** and 40 nM **HP1**. In the initial design phase, the buffer condition of 1× PBS (pH 7.4) and 10 mM $MgCl_2$ was used. The buffer condition was refined as 1× PBS (pH 7.4) and 5 mM $MgCl_2$ (Supplementary Figure S1) for the subsequent in-depth studies with the shortlisted **HP-I1** designs (Figure 4 onwards).

The elongated associative toehold design was implemented on other common readout moieties, namely molecular beacon, X-Probe and linear fluorophore-quencher (F-Q) systems. The molecular beacon was snap cooled as per the preparation of HCR hairpins. The X-probe complex were prepared by mixing 2:1.5:1.2:1 molar ratio of strand 3:1:2:4 (sequences of the 4 strands are listed in Supplemen-

tary Table S2) on the basis of 1 μM of X-Probe strand 4. The F–Q complex was prepared by mixing the fluorophore and quencher strands in 1:1.5 molar ratio on the basis of 1 μM fluorophore strand. Both the X-probe and F-Q complexes were heated in 1× PBS (pH 7.4) and 5 mM $MgCl_2$ to 95°C for 5 min and slowly cooled to room temperature at a controlled rate of −0.2°C/s.

Fluorescence measurement for HCR-FRET readout

Hybridization chain reaction (HCR) was used to generate the readout signal. All reactions proceeded at room temperature for a reaction volume of 20 μl in the 384-well black plate. Split target (**ST**) of the desired concentration was first added to each well, followed by the one-pot addition of the SPC mixture to a final reaction concentration of 40 nM for **HP1** and 20 nM for **HP2**, **I1/HP-I1** and **I2** under the optimized buffer condition of 1× PBS (pH 7.4) and 5 mM $MgCl_2$.

The FRET readout was measured on a microplate reader (Tecan Spark 10M). The z-position and gain was optimized using the i-control software tool for each set of DNA readout concentration and kept constant throughout the analysis. An excitation wavelength of 495 nm was used and the fluorescence intensity of **HP2**-Cy3 and **HP1**-Cy5 was measured at 560 and 665 nm emission wavelength. For kinetics study, the fluorescence measurement was performed every 5 min for a total analysis time of 3 h at room temperature. We quantified the readout signal as FRET ratio, which was calculated by dividing the fluorescence intensity of **HP1**-Cy5 by that of **HP2**-Cy3 (after baseline correction with a buffer blank for each fluorescence reading).

We calculated the signal-to-noise ratio (S/N) by dividing the mean FRET signal in the presence of **ST** target by that without **ST**. The circuit kinetics (rate of change of signal generation) was estimated by taking the gradient of the initial, linear portion (up to $t = 20$ min point) of the kinetics trace. This did not take into account any kinetic model but sufficed in providing a quantitative sense of the relative change in rate of signal generation by incorporating the hairpin lock design. We calculated the limit of detection (LOD) as the **ST** concentration generating a FRET signal of mean + 3 S.D. of the negative control (0 nM **ST**).

RESULTS AND DISCUSSION

Design considerations of hairpin lock

As with any circuit design, the foremost consideration is to minimize circuit leakage (20–22). In the proposed design, this depended on whether the hairpin lock was able to protect the elongation domain *e* from exposing itself in absence of the target. Different combinations of domains *a, e* and b_2* in **HP-I1** were compared in Figure 2. We denoted the designs as: *A*—'length of associative domain (*a*)'—'length of elongation domain (*e*)'—'length of clamp domain (b_2*)'. Starting from a length of 4 nt domain *a*, an equal length of domain *e* was added which was also the minimal stem length for a stable hairpin design at room temperature (23). Extensive leakage was observed (A440) which did not subside (A431) until 2 nt of domain *e* was replaced with a 2 nt clamp formed partially by the original toehold domain *b*

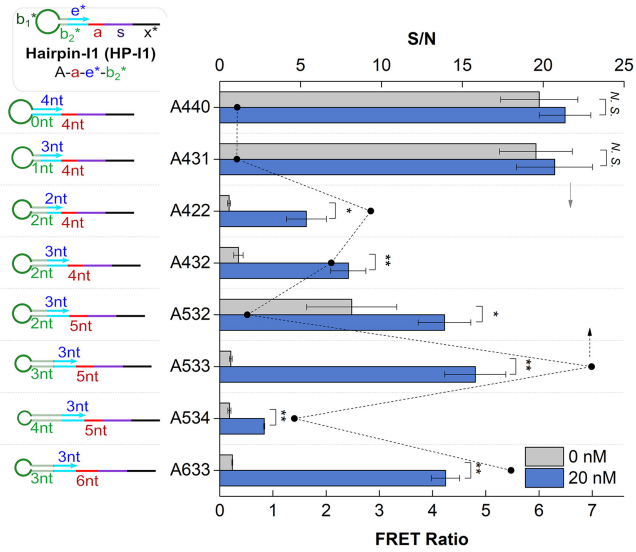

Figure 2. Comparison of HCR FRET ratio (bar charts) obtained for different design configurations of hairpin initiator 1 (**HP-I1**, sequences are listed in Supplementary Table S1). The lengths of domains b_2, *e* and *a* for each **HP-1** design are indicated in green, blue and red respectively to the left of the graph. Grey bars represent no target added while blue bars represent addition of 20 nM split target (**ST**). Data are presented as mean ± standard deviation at $t = 1$ h. The signal-to-noise ratio (S/N) data are presented as a line-and-scatter plot. N.S. not significant; * $P < 0.05$; ** $P < 0.01$ (one-sided Student's *t*-test).

as domain b_2* (A422). Based on NUPACK analysis (19), a large fraction of **'HP-I1'-I2** complex formed even in absence of **ST** which was likely to be the main source of leakage in designs A440 and A431.

The clamp domain b_2* was necessary to stabilize the 'closed' hairpin state, similar to what we and others have previously observed (16,17). In this context, the clamp served as a buffer domain to avoid depending solely on domain *e* to balance between the 'opened' (after elongation) and 'closed' (as hairpin lock) state, which left no freedom for design and was experimentally proven to be detrimental for circuit leakage as seen in A440. It was necessary to use part of the toehold domain *b* as the clamp domain to avoid introducing additional gaps between the trigger domains *c** *b** upon association (Figure 1). It was important to balance the lengths of domains b_2* and *e*. Keeping the clamp length as 2 nt, a longer 3 nt domain *e* led to increased leakage and hence drop in signal-to-noise ratio (S/N) as seen in design A432.

We next investigated if the presence of a hairpin lock in **I1** would serve as a sufficiently strong energetic barrier to reduce leakage for longer association lengths. When the association length increased to 5 nt (A532), the leakage worsened significantly. However, when the clamp length was further increased by 1 nt (A533), the leakage was significantly reduced to give a comparable S/N ratio to the best 4 nt association length design (A422). This showed that an optimized hairpin lock design with the appropriate clamp length allowed longer association lengths to be used which was previously not feasible due to high leakage (15).

We further increased the clamp length to 4 nt (A534) which led to a significant drop in signal and leak. This was

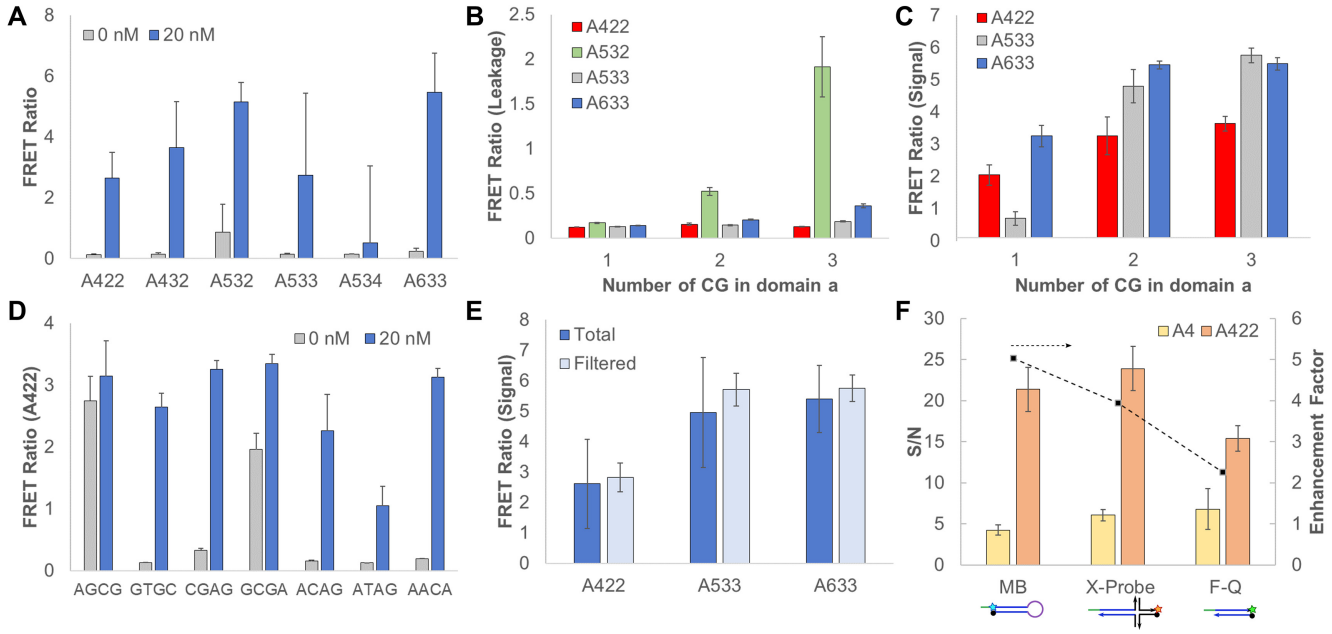

Figure 3. (**A**) Six feasible hairpin initiator 1 (**HP-I1**) designs were further evaluated. Two additional sequences were generated for each domain configuration. The HCR FRET signal (when 20 nM of **ST** were added) and noise (0 nM **ST** present) are presented as mean ± standard deviation of a total of three sequence designs at t = 1 h. The large standard deviation suggests that domain length was insufficient for defining the system. (**B**) The leakage, that is, FRET ratio obtained in presence of 0 nM **ST**, for four domain configurations showed an increasing trend as the the number of CG in domain *a* increased. (**C**) The signal, that is, FRET ratio obtained in presence of 20 nM **ST**, for three domain configurations also showed similar positive correlation with an increase in number of CG in domain *a*. (**D**) Contiguous stretch of three CG was detrimental for leakage; while contiguous stretch of three AT resulted in poor signal generation. (**E**) By filtering off sequences with contiguous stretch of three CG or AT, the standard deviation (out of a set of six to eight sequences) for each domain configuration was significantly reduced. (**F**) The hairpin lock design was found to be generally applicable for other readout moieties including molecular beacon (MB), X-probes and linear fluorophore-quencher (F-Q) besides the HCR FRET used for this work.

within expectation since the clamp domain favoured only the 'closed' state and so a longer length would impede the hairpin opening step. It was possible to balance the effect of long clamp domain using longer elongation domain; however, this meant that **HP-I1** would have an excessively long stem length which instead hindered the overall circuit kinetics (Supplementary Figure S2). As such, the elongation domain *e* was capped at 3 nt for the rest of the study since it was not effective to have exceedingly long toehold (24); while the clamp length was kept at 2–3 nt.

Generalizability of hairpin lock design

Having established the design framework at the domain level, here we demonstrated its generalizability at the sequence level (all sequences are listed in Supplementary Table S2). Two more random sequences for each of the six feasible domain configurations identified in Figure 2 were generated using NUPACK. The general trends observed at the domain level remained (Figure 3A), that is, relatively high leakage was obtained for weak A532 hairpin lock while the signal was greatly subdued with strong A534 hairpin locks. The large standard deviation for each design suggests significant dependence on specific sequence design which we next studied in greater details.

We previously reported that the domain level design can be broken down into domain length and number of CG (18). All randomly generated sequences were range-bound in terms of its number of CG, that is, one to three CGs for domain *a* and more than two CGs for domain *e*. In another words, NUPACK analysis predicted that the system would leak if either domain *a* had too high CG content or domain *e* (which was part of the hairpin lock) was not strong enough. Four out of six of the domain configurations were represented by sequences spanning the entire range of CG content in domain *a* (Figure 3A). Generally, as the number of CG increased, the leakage increased and this was most evidently observed for A532 which was a weak hairpin lock design (Figure 3B). On the other hand, the signal generation was also boosted as the number of CG increased (Figure 3C). Note that A532 was eliminated from this analysis as its leakage was too high for the signal to be compared meaningfully.

Next, we focused on A422 and generated more sequence permutations to further distil possible trends from sequence position and identity (Figure 3D). For the sequences containing three CGs in domain *a*, exceptional levels of leakage was observed in two cases, that is, AGCG and GCCA. This suggests that a contiguous region of three CG should be avoided. On the other hand, the signal generated from ATAG was noticeably lower than AACA despite both sequences having one CG, suggesting that a contiguous region of three AT should be avoided as well.

We generalized that the feasible design space could be defined at the domain level, both in terms of length and number of CG. The specific sequence design can be further refined by considering the relative positions of either CG or AT nucleotides. By eliminating the extreme cases (contiguous stretch of three or more CG or AT), we were able to filter our randomly generated sequences into smaller subsets

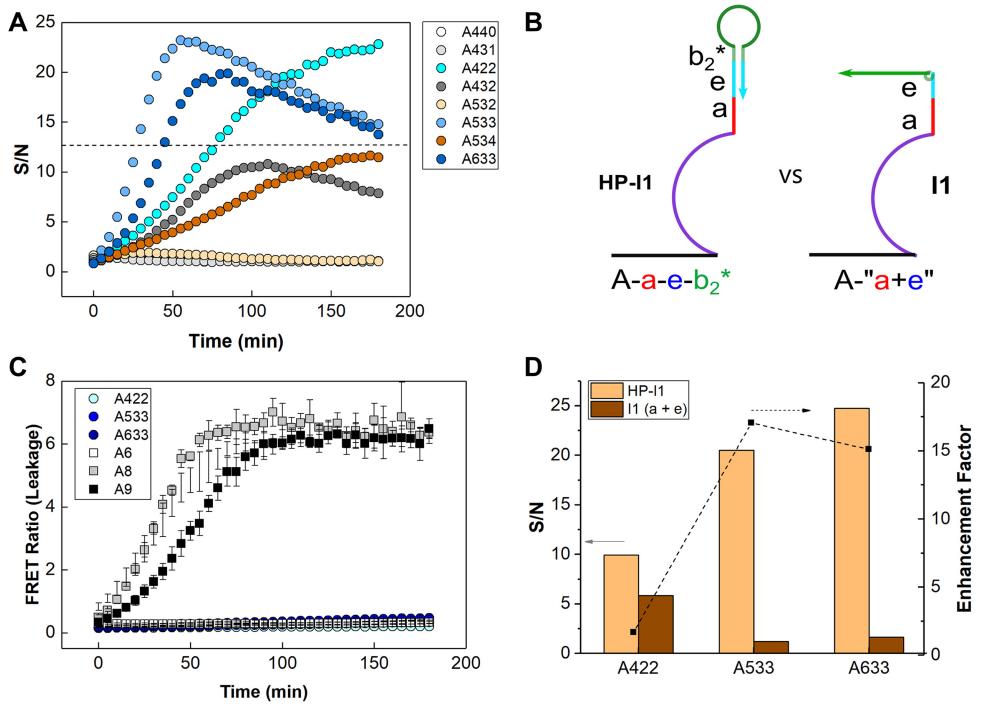

Figure 4. (**A**) Signal-to-noise ratio (S/N) for different hairpin initiator 1 (HP-I1) designs was calculated by dividing the mean HCR FRET signal in presence of 20 nM **ST** target by that of 0 nM **ST**. An arbitrary cut-off line was drawn to guide the eye to the two tiers of S/N; high S/N was attained by designs A422, A533 and A633 which were shortlisted for further investigation. (**B**) Schematics to illustrate that the two initiator designs compared in (**C**) and (**D**) were the hairpin initiator (**HP-I1**) and linear initiator (**I1**) with an equivalent elongated association length. (**C**) Evolution of circuit leakage when the respective initiators were reacted in absence of the target. **HP-I1** could suppress the leakage significantly compared to **I1** across all association lengths (domain *a*). Data are presented as mean ± standard deviation. (**D**) The S/N of the **HP-I1** design was higher than the linear **I1** design for all association lengths tested at $t = 1$ h (bar chart). Having a hairpin lock design in the initiator enhanced the S/N by two- to seventeen-fold compared to the linear **I1** design.

with noticeably reduced variations, i.e. coefficient of variation (CV) <10% (Figure 3E).

To further demonstrate the generalizability of the hairpin lock design, we implemented the A422 elongated associative toehold on other common readout moieties, that is, molecular beacon (25), X-Probe (26) and linear fluorophore–quencher (F–Q). In all three cases, the S/N achieved from our elongated associative toehold design was higher than the conventional associative toehold with an enhancement factor (defined as the ratio of the respective S/N) ranging between 2 and 5 (Figure 3F).

Hairpin lock reduced circuit leakage

The best **HP-I1** designs from this study, that is, A422, A533 and A633, were shortlisted based on their superior S/N ratio (Figure 4A) for a more thorough study using one representative sequence per HP-I1 design (Supplementary Table S1). We first compared the extent of leakage and its impact on S/N ratio between the **HP-I1** and its equivalent elongated association length (domain *a* + *e*) in the linear **I1** design, which we denoted as A—'length of associative domain' (Figure 4B). Here, leakage referred to the signal generated from **'HP-I1'-I2** complex in absence of **ST**, which was mediated by hybridization at the exposed association region (either domain *a* in **HP-I1** or domain *a* + *e* in **I1**).Tremendous leakage was observed for long association lengths of 8 nt and 9 nt exposed in the linear **I1** which was suppressed drastically using the equivalent **HP-I1** design (Figure 4C). This translated into significantly improved S/N ratio, that is, by 2- to 17-fold (depending on the exact domain design) simply by incorporating the hairpin lock into the **I1** design (Figure 4D).

Hairpin lock improved kinetics and signal generation

Next, we evaluated if the hairpin initiator could improve the overall circuit kinetics and thermodynamics in spite of having an additional kinetic step of having to open the hairpin lock in **HP-I1**. The FRET signal evolution of **HP-I1** (domain $a \rightarrow a + e$) was compared with the linear **I1** design with either the initial (domain *a* only) or elongated (domain *a* + *e*) association length (Figure 5A).

The **HP-I1** design clearly outperformed the linear **I1** design with the initial shorter association length (Figure 5B–D). The signal generated by the end of 3 h increased by 2- (A633) to 11-fold (A533) while the overall reaction rate was enhanced by at least 4-fold. The equilibrium signal approached close to that of the linear **I1** initiator with an elongated association length, which indicated that this dynamic elongation of the associative toehold effectively tuned the circuit thermodynamics towards a more favourable state This was within expectation as the **ST-'HP-I1'-I2** (Figure 1C) assembly was almost equivalent in both designs except for the domain *e** overhang in **HP-I1**. However, the circuit kinetics was indeed slightly penalized (by about 10–20%)

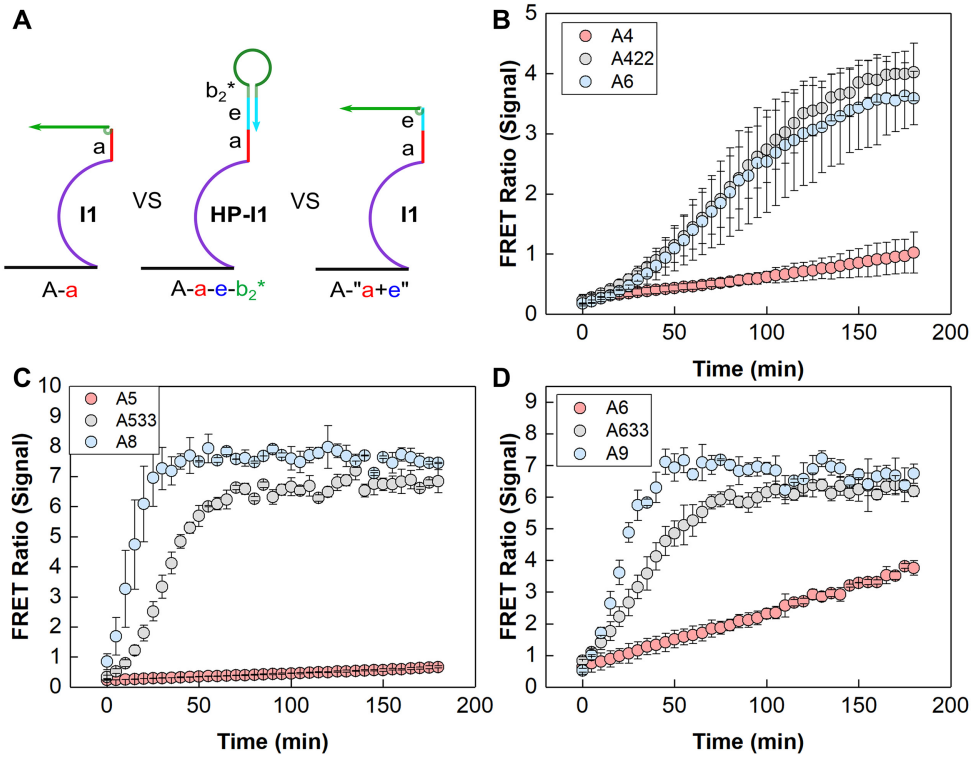

Figure 5. (**A**) The performance of the hairpin initiator (**HP-I1**) design (domain $a \rightarrow a + e$) was compared to the linear initiator (**I1**) design with an association length before (domain a only) and after elongation (domain $a + e$). 20 nM **ST** was added. The **HP-I1** design improved the kinetics and thermodynamics of SPC compared to the linear **I1** design with the initial association length, and approached close to the performance of that with elongated association length for the **HP-I1** designs of (**B**) A422, (**C**) A533 and (**D**) A633. All data are shown as mean ± S.D. ($n = 3$) of the HCR FRET signal.

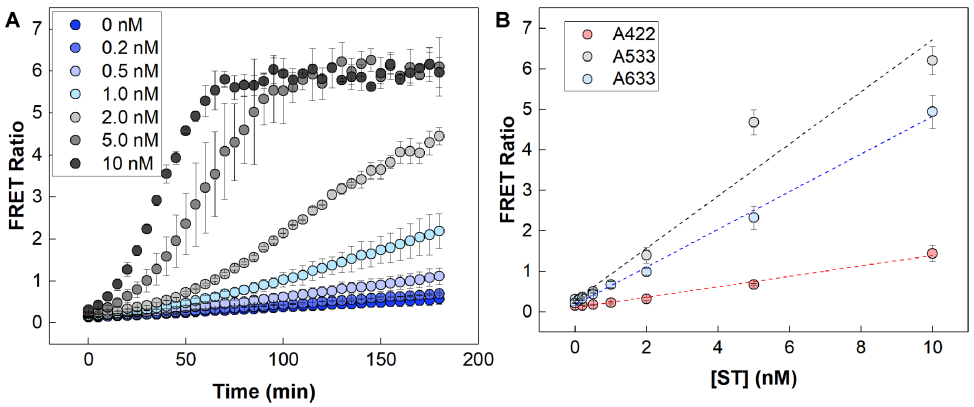

Figure 6. (**A**) Kinetics of HCR FRET signal generation for A633 hairpin initiator design when titrated with 0–10 nM of split target (**ST**). (**B**) The FRET ratio taken at $t = 1$ h depended linearly on the **ST** concentration for A422 (red), A533 (gray) and A633 (blue) designs. All data are shown as mean ± S.D. ($n = 3$).

when compared to the linear **I1** design with the elongated association length due to the additional step of having to open the hairpin lock. This penalty was more apparent for longer lengths of domains e and b_2 due to the presence of a more stable hairpin lock which posed a stronger kinetic barrier for the hairpin opening step. Nonetheless, it was apparent that the gain in circuit kinetics as a result of elongating the associative domain was more prominent than this slight penalty imposed by the hairpin lock to achieve the nett gain in the overall circuit kinetics (>400% improvement).

Improved analytical performance of DNA circuit

We characterized the analytical performance of the hairpin initiator design to assess if its superior kinetics and thermodynamics could be translated into analytically useful metrics for SPC. While SPC was previously reported to be highly specific for discriminating point mutations, its analytical sensitivity still has room for improvement (27).The FRET signal generated from the modified SPC was clearly dependent on the concentration of **ST** titrated (Figure 6A).

Table 1. Comparison of the limit of detection (LOD) achieved at $t = 1$ h between the linear initiator 1 (**I1**) and hairpin initiator 1 (**HP-I1**) designs. The shorter initial association length was used in the **I1** system

	LOD (nM)			
Associative domain	I1	R^2	HP-I1	R^2
A422 (4 nt → 6 nt)	0.791	0.978	0.393	0.992
A533 (5 nt → 8 nt)	1.17	0.936	0.170	0.953
A633 (6 nt → 9 nt)	1.67	0.984	0.144	0.996

Linear dosage relationship was observed for the concentration range ca. 0.2–10 nM (Figure 6B). This dynamic range was in line with our previous study on hybridization chain reaction (HCR) which was used as the readout signal in this work (28).

The limit of detection (LOD) of the **HP-I1** design was compared to the linear **I1** design with a shorter initial associative domain after 1 h of reaction which, on average, was improved by an order of magnitude (Table 1). Note that it was not meaningful to compare with the elongated associative domain due to the extensive amount of leakage in that system. Interestingly, we noticed that the LOD improved marginally with increasing association length in the **HP-I1** design which would otherwise be detrimental in the linear **I1** design due to the increased leakage with longer association length (15,29–31).

The improved performance could be attributed primarily to the enhanced circuit kinetics which enabled a substantially stronger FRET signal to be generated rapidly over the much slower leak reaction hence improving the circuit S/N ratio which could now be achieved within a shorter reaction time. The caveat with attaining equilibrium signal within a much shorter reaction time is that analysis should be kept short (within an hour); otherwise the boost in S/N ratio due to the improved kinetics and thermodynamics could be eroded by the gradual increase in circuit leakage. The enhanced performance within a shorter time is nonetheless an advantageous feature for most applications that we can think of and particularly for detection-related work.

CONCLUSION

In conclusion, we introduced the concept of an elongated associative toehold and demonstrated its effectiveness in improving the overall circuit kinetics and thermodynamics by enabling a longer associative domain to be used without incurring high circuit leak rate. A detailed study was carried out to understand the contributions from each additional domain of this modified design which culminated in a set of design guidelines. Three hairpin-locked initiator designs (**HP-I1**) with elongated association lengths of A422 (4 → 6 nt), A533 (5 → 8 nt) and A633 (6 → 9 nt) were compared against the linear initiator designs. We demonstrated that the elongated associative toehold design boosted the equilibrium signal (relative to the shorter initial association lengths) by at least 2-fold with its kinetics approaching close to that of the respective elongated association lengths while a well-designed hairpin lock was effective in suppressing the circuit leakage. This translated to an improved signal-to-noise ratio (S/N) and hence better analytical performance with improved limit of detection and faster detection speed as demonstrated on the SPC system. We anticipate that this hairpin lock concept can generally be applied for other split trigger designs and associative toehold-mediated displacement reactions.

SUPPLEMENTARY DATA

Supplementary Data are available at NAR Online.

FUNDING

Singapore Ministry of Education Academic Research Fund Tier 2 [MOE2019-T2-1-116]. Funding for open access charge: Singapore Ministry of Education Academic Research Fund Tier 2 [MOE2019-T2-1-116].
Conflict of interest statement. None declared.

REFERENCES

1. Yurke,B., Turberfield,A.J., Mills,A.P., Simmel,F.C. and Neumann,J.L. (2000) A DNA-fuelled molecular machine made of DNA. *Nature*, **406**, 605.
2. Zhang,D.Y. and Seelig,G. (2011) Dynamic DNA nanotechnology using strand-displacement reactions. *Nat. Chem.*, **3**, 103.
3. Hu,P., Li,M., Wei,X., Yang,B., Li,Y., Li,C.-Y. and Du,J. (2018) Cooperative toehold: a mechanism to activate DNA strand displacement and construct biosensors. *Anal. Chem.*, **90**, 9751.
4. Zhu,J., Zhang,L., Zhou,Z., Dong,S. and Wang,E. (2014) Molecular aptamer beacon tuned DNA strand displacement to transform small molecules into DNA logic outputs. *Chem. Commun.*, **50**, 3321.
5. Green,S.J., Lubrich,D. and Turberfield,A.J. (2006) DNA hairpins: fuel for autonomous DNA devices. *Biophys. J.*, **91**, 2966.
6. Genot,A.J., Zhang,D.Y., Bath,J. and Turberfield,A.J. (2011) Remote toehold: a mechanism for flexible control of DNA hybridization kinetics. *J. Am. Chem. Soc.*, **133**, 2177.
7. Chen,X. (2012) Expanding the rule set of DNA circuitry with associative toehold activation. *J. Am. Chem. Soc.*, **134**, 263.
8. Genot,A.J., Bath,J. and Turberfield,A.J. (2013) Combinatorial displacement of DNA strands: application to matrix multiplication and weighted sums. *Angew. Chem. Int. Ed.*, **125**, 1227.
9. Tang,Y., Wang,Z., Yang,X., Chen,J., Liu,L., Zhao,W., Le,X.C. and Li,F. (2015) Constructing real-time, wash-free, and reiterative sensors for cell surface proteins using binding-induced dynamic DNA assembly. *Chem. Sci.*, **6**, 5729.
10. Ang,Y.S., Li,J.E.J., Chua,P.-J., Ng,C.-T., Bay,B.-H. and Yung,L.-Y.L. (2018) Localized visualization and autonomous detection of cell surface receptor clusters using DNA proximity circuit. *Anal. Chem.*, **90**, 6193.
11. Li,F., Lin,Y. and Le,X.C. (2013) Binding-induced formation of DNA three-way junctions and its application to protein detection and DNA strand displacement. *Anal. Chem.*, **85**, 10835.
12. Deng,B., Chen,J. and Zhang,H. (2014) Assembly of multiple DNA components through target binding toward homogeneous, isothermally amplified, and specific detection of proteins. *Anal. Chem.*, **86**, 7009.
13. Choi,H.M.T., Schwarzkopf,M., Fornace,M.E., Acharya,A., Artavanis,G., Stegmaier,J., Cunha,A. and Pierce,N.A. (2018) Third-generation in situ hybridization chain reaction: multiplexed, quantitative, sensitive, versatile, robust. *Development*, **145**, dev165753.
14. Li,F., Tang,Y., Traynor,S.M., Li,X.-F. and Le,X.C. (2016) Kinetics of proximity-induced intramolecular DNA strand displacement. *Anal. Chem.*, **88**, 8152.
15. Ang,Y.S., Tong,R. and Yung,L.-Y.L. (2016) Engineering a robust DNA split proximity circuit with minimized circuit leakage. *Nucleic Acids Res.*, **44**, e121.
16. Wang,B., Thachuk,C., Ellington,A.D., Winfree,E. and Soloveichik,D. (2018) Effective design principles for leakless strand displacement systems. *Proc. Natl. Acad. Sci. U.S.A.*, **115**, E12182.

17. Ang,Y.S. and Yung,L.-Y.L. (2014) Engineering self-contained DNA circuit for proximity recognition and localized signal amplification of target biomolecules. *Nucleic Acids Res.*, **42**, 9523.
18. Ang,Y.S. and Yung,L.-Y.L. (2016) Rational design of hybridization chain reaction monomers for robust signal Amplification. *Chem. Commun.*, **52**, 4219.
19. Zadeh,J.N., Steenberg,C.D., Bois,J.S., Wolfe,B.R., Pierce,M.B., Khan,A.R., Dirks,R.M. and Pierce,N.A. (2011) Nupack: analysis and design of nucleic acid systems. *J. Comput. Chem.*, **32**, 170.
20. Yin,P., Choi,H.M.T., Calvert,C.R. and Pierce,N.A. (2008) Programming biomolecular self-assembly pathways. *Nature*, **451**, 318.
21. Jiang,Y.S., Bhadra,S., Li,B. and Ellington,A.D. (2014) Mismatches improve the performance of strand-displacement nucleic acid circuits. *Angew. Chem. Int. Ed.*, **53**, 1845.
22. Zhang,D.Y. (2011) In: Sakakibara,Y. and Mi,Y. (eds). *DNA Computing and Molecular Programming: 16th International Conference, DNA 16, Hong Kong, China, June 14–17, 2010, Revised Selected Papers*. Springer Berlin Heidelberg, Berlin, Heidelberg, pp. 162.
23. Zuker,M. (2003) Mfold web server for nucleic acid folding and hybridization prediction. *Nucleic Acids Res.*, **31**, 3406.
24. Zhang,D.Y. and Winfree,E. (2009) Control of DNA strand displacement kinetics using toehold exchange. *J. Am. Chem. Soc.*, **131**, 17303.
25. Tyagi,S. and Kramer,F.R. (1996) Molecular beacons: probes that fluoresce upon hybridization. *Nat. Biotechnol.*, **14**, 303.
26. Wang,J.S. and Zhang,D.Y. (2015) Simulation-guided DNA probe design for consistently ultraspecific hybridization. *Nat. Chem.*, **7**, 545.
27. Ang,Y.S., Lai,P.S. and Yung,L.-Y.L. (2020) Design of split proximity circuit as a plug-and-play translator for point mutation discrimination. *Anal. Chem.*, **92**, 11164.
28. Dirks,R.M. and Pierce,N.A. (2004) Triggered amplification by hybridization chain reaction. *Proc. Natl. Acad. Sci. U.S.A.*, **101**, 15275.
29. Li,F., Zhang,H., Wang,Z., Li,X., Li,X.-F. and Le,X.C. (2013) Dynamic DNA assemblies mediated by binding-induced DNA strand displacement. *J. Am. Chem. Soc.*, **135**, 2443.
30. Li,F., Zhang,H., Lai,C., Li,X.-F. and Le,X.C. (2012) A molecular translator that acts by binding-induced DNA strand displacement for a homogeneous protein assay. *Angew. Chem. Int. Ed.*, **51**, 9317.
31. Teichmann,M., Kopperger,E. and Simmel,F.C. (2014) Robustness of localized DNA strand displacement cascades. *ACS Nano*, **8**, 8487.